Journal Name

ARTICLE

Shining light on the antenna chromophore in lanthanide based dyes

Received 00th January 20xx,
Accepted 00th January 20xx

DOI: 10.1039/x0xx00000x

www.rsc.org/

Anne Kathrine R. Junker,[a] Leila R. Hill,[b] Amber L. Thompson,[b] Stephen Faulkner*[b] and Thomas Just Sørensen*[a]

Lanthanide based dyes and assays exploit the antenna effect, where a sensitiser-chromophore is used as a light harvesting antenna and subsequent excited state energy transfer populates the emitting lanthanide centred excited state. A rudimentary understanding of the design criteria for designing efficient dyes and assays based on the antenna effect is in place. By preparing kinetically inert lanthanide complexes based on the DO3A scaffold, we are able to study the excited state energy transfer from a 7-methoxy-coumarin antenna chromophore to europium(III) and terbium(III) centred excited states. By contrasting the photophysical properties of complexes of metal centres with and without accessible excited states, we are able to separate the contributions from the heavy atom effect, photoinduced electron transfer quenching, excited state energy transfer and molecular conformations. Furthermore, by studying the photophysical properties of the antenna chromophore, we can directly monitor solution structure and are able to conclude that excited state energy transfer from the chromophore singlet state to the lanthanide centre does occur.

Introduction

Lanthanide luminescence is characterised by uniquely narrow emission bands, long excited state lifetimes and relatively environmentally invariant emission spectra.[1-3] These unique features arise due to the forbidden nature of *f-f* transitions, but come with a cost of very low molar absorption coefficients.[4] Therefore, direct excitation into the lanthanide centred excited state is in the best case around a million times less efficient than that for standard organic fluorescent dyes.[5, 6] Despite this apparent downside, lanthanide luminescence gives rise to background-free images, highly sensitive binding and high-content screening assays.[7-22]

These applications exploit the antenna effect, where an organic chromophore is used as a sensitiser for lanthanide centred luminescence.[23-42] The antenna chromophore absorbs light with a high molar absorptivity, and transfers the excited state energy to the lanthanide centre that subsequently emits, see Figure 1. The chromophore typically has a molar absorptivity in the range from 5,000 to 50,000 $M^{-1}cm^{-1}$, which despite the introduction of an energy transfer step of limited efficiency, gives rise to an improved brightness of the lanthanide based dye. As the antenna chromophore can absorb, where the lanthanide ion does not, close to perfect signal-to-background can be achieved in time-gated assays based on sensitised lanthanide luminescence.[8, 15, 17] For imaging, the use of lanthanide based dyes has been limited by excitation in the UV.[3, 7, 12, 19] This limitation has been circumvented using two-photon excitation and by using dyes with more than one antenna chromophore.[43-45]

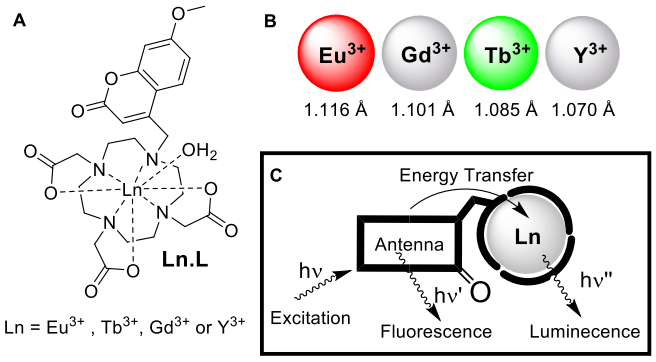

Figure 1. (**A**) Molecular structure of the investigated complexes **Ln.L**, (**B**) A scaled representation of the ionic radius of the europium(III), gadolinium(III), terbium(III), and yttrium(III) ions.[46] (**C**) A schematic representation of the antenna effect.

Efficient dyes have been developed for commercial assays,[8, 47] and for use in luminescence microscopy.[18, 19] These follow established guidelines that are based on the assumption that the excited state energy transfer occurs from the antenna chromophore's lowest excited triplet state and via the Dexter mechanism.[3, 27, 38, 48] Therefore, the chromophore must be in contact with the lanthanide ion, ideally coordinating to the metal centre, for the energy transfer to occur. Bearing in mind that lanthanide based dyes are used in solutions with

[a] Nano-Science Center & Department of Chemistry, University of Copenhagen, Universitetsparken 5, 2100 København Ø, Denmark. TJS@chem.ku.dk
[b] Chemistry Research Laboratory, University of Oxford, 12 Mansfield Road, Oxford OX1 3TA, United Kingdom. stephen.faulkner@chem.ox.ac.uk

Electronic Supplementary Information (ESI) available: The ESI include synthetic procedures, data from compound characterisation, NMR spectra, absorption spectra, time-resolved emission decay profiles, time gated emission spectra, steady-state emission and excitation spectra, and structural information in CIF format. See DOI: 10.1039/x0xx00000x

Please do not adjust margins

competitive ligands, evaluating the solution structure around the lanthanide ion is a prerequisite for unravelling the physicochemical properties of the complex.[49-51]

With the antenna chromophore guidelines,[3, 27, 38] we can start designing efficient lanthanide based dyes, but there is still vital information missing. Thus, the current solution is to build large libraries of antenna chromophores and test the resulting library of lanthanide based dyes.[38, 52-54] This requires a large effort as each antenna chromophore must be tested with several lanthanide(III) ions. Rather than performing a screening, we aim to rationalise the physicochemical properties thereby enabling design lanthanide based dyes.

Figure 1 shows the complexes we used to investigate the antenna principle in detail. A 1,4,7,10-tetraazadodecane-1,4,7-triacetic acid (DO3A) ligand with a 4-methyl-7-methoxy-coumarin as the fourth pendant arm was synthesised, and complexes of yttrium(III) **Y**.**L**, europium(III) **Eu**.**L**, gadolinium(III) **Gd**.**L**, and terbium(III) **Tb**.**L** were made in significant quantities. We recently showed that the curium(III) complex **Cm**.**L** of this ligand gave rise to direct perturbation of the ligand chromophore by the 5*f* orbitals.[55] **Cm**.**L** was contrasted to the complexes of europium(III) and terbium(III), and all three were shown to be kinetically inert with stability constants in HEPES buffer around 10^{28}. **Eu**.**L** was shown to have a lower stability constant and higher hydration number *q* than **Cm**.**L** and **Tb**.**L**; a surprising fact that we will treat in detail here.[55]

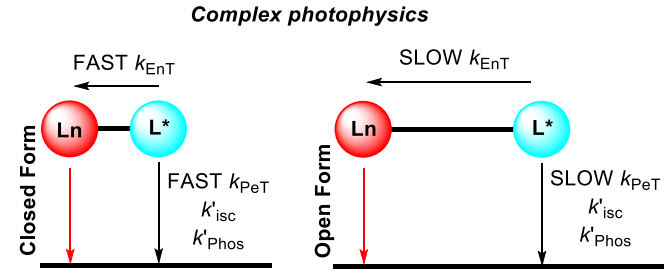

Figure 2. The two complex modes in solution; Left: The closed form where the Ln centre and antenna are in close proximity, enabling fast energy transfer and fast deactivation of the excited antenna state. Right: The open form where the Ln centre and antenna are far from each other, resulting in slow energy transfer and slow deactivation of the antenna excited state.

We have started to explore the perturbation caused by lanthanide(III) ions to the excited state properties of organic chromophores by studying them in collision quenching conditions.[56-58] The one conclusion reached so far is that studying model systems will not reveal the detailed photophysics of lanthanide based dyes. Therefore, we now scrutinize the antenna- and lanthanide centred photophysics when the lanthanide(III) ion and chromophore are in the same complex. While two forms of the **Ln**.**L** complexes are expected to be present in solution, the complexity of the investigated system is greatly reduced when compared to two freely diffusing units.[56] Figure 2 shows the two forms—designated open and closed—and the expected effect the solution structure will have on the excited energy transfer processes. Note that the induced inter-system crossing and phosphorescence is treated as a medium effect and is not dependent on solution structure.

By contrasting the solution structure and photophysics of six compounds: **Y**.**L**, **Eu**.**L**, **Gd**.**L**, **Tb**.**L**, H_3.**L**, and H_5.L^{2+} using ^{1}H NMR and optical spectroscopy, we can confirm that two forms (open and closed, Figure 2) describe the solution structure of these complexes. We can confirm that the europium(III) complex differs in both solution structure and photophysics from the other metal complexes. In addition, we can separate the four distinct excited state processes introduced in the antenna chromophore by the metal ions. Here, we focus on the ligand-centred singlet excited state and the first step of the excited state energy transfer cascade that leads to the lanthanide(III) centred excited state.

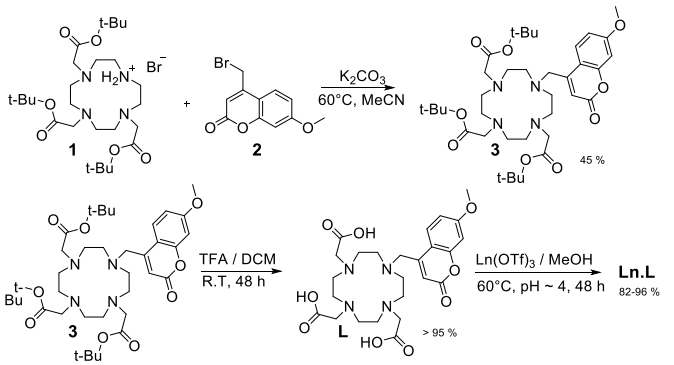

Scheme 1. Synthetic pathway to ligand **L** and lanthanide complexes **Ln.L**. Ln = Y^{3+}, Eu^{3+}, Gd^{3+}, and Tb^{3+}.

Results and Discussion

Synthesis and Characterisation

The complexes were synthesised in three steps from 1,4,7,10-tetraazacyclododecane or cyclen. The first step is a chemoselective alkylation of three of the four amines using *t*-butyl bromoacetate. Steric congestion and the very different solubility in toluene of the tetraalkylated byproduct and the bromide salt of the tri-alkylated cyclen **1** allowed it to be isolated in a good yield on a multigram scale.[59] In our hands, the reaction runs well using up to 0.1 mol of cyclen. On a larger scale reaction, the yield is reduced to <50 %. The trialkylated cyclen also known as DO3A-triester **1**, is the readily available starting material for functionalised DO3A (1,4,7,10-tetraazacyclododecane-1,4,7-triacetic acid) ligands. The synthetic route to the studied lanthanide complexes are shown in Scheme 1. The fourth cyclen amine in triester **1** was alkylated with 4-bromomethyl-7-methoxy-coumarin **2** in acetonitrile at 60°C. The resulting product **3** was isolated using column chromatography in an acceptable yield. The ester of the proligand **3** was cleaved using trifluoroacetic acid in dichloromethane, and upon trituration with diethyl ether from methanol the ligand H_3.**L** was isolated as a pale yellow powder.

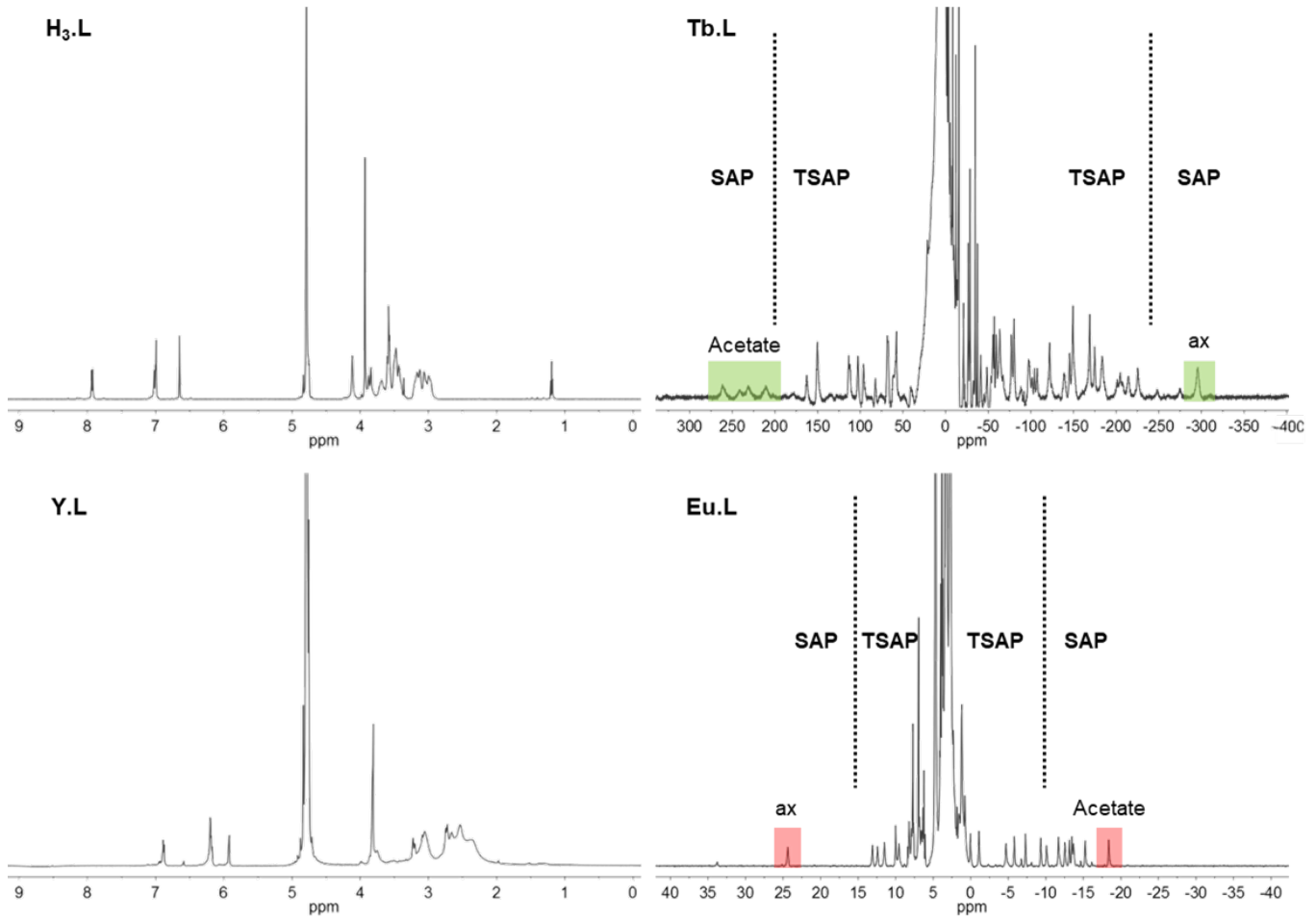

Figure 3. ^{1}H NMR spectra of the free ligand H_3.**L** and the lanthanide complexes **Ln.L** in D_2O. The spectrum of the free ligand were obtaind at pH ~ 4, and at pH 7 for the complexes. On the spectra lanthanide complexes the regions corresponding to the SAP and TSAP conformers are indicated based on the corresponding Ln.DOTA complexes, and the resonances corresponding to the axial and acetate arm protons are highlighted.

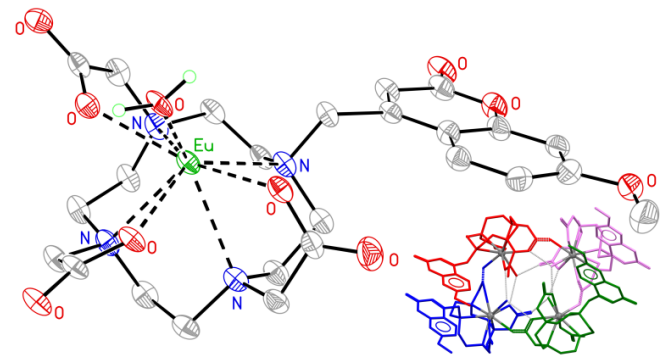

Figure 4. Displacement ellipsoid plot for the orthorhombic polymorph of **Eu.L** drawn at 20% probability. The main picture shows one formula unit with selected hydrogen atoms and NaOTf omitted for clarity. In the solid state, **Eu.L** forms tetramers held together by hydrogen bonding between the apical water and ligand acetate moieties (shown inset), a feature seen in all three structures studied.

The complexes of yttrium(III), europium(III), gadolinium(III) and terbium(III) were formed from the corresponding triflate salts in methanol at pH 4. The complexes were isolated upon removal of excess lanthanide ions as a mixed hydroxide precipitate formed at pH 10. All compounds were characterized using ^{1}H NMR and high-resolution mass spectrometry.

Figure 3 shows the ^{1}H NMR spectra of the free ligand H_3.**L** and the **Y**.**L**, **Eu**.**L**, and **Tb**.**L** complexes. Note that it is not possible to obtain a ^{1}H NMR spectrum of the **Gd**.**L** complex, a consequence of the rapid relaxation protons held in close proximity to Gd^{3+}, an f^7-ion.[60] While the ^{1}H NMR spectra of the ligands are pH dependent, the ^{1}H NMR spectra of the complexes do not change with pH, although the complexes precipitate at low pH.

For **Eu**.**L**, we were able to confirm the constitution of the complexes using single crystal X-ray diffraction, see ESI for details. The crystal structure consists of tetramers of **Eu**.**L**, where each europium(III) cation is encapsulated by the ligand and bridged by the carboxylate pendant arms from a neighbouring complex. The coordination sphere of europium(III) is thus filled with seven donor atoms from the ligand, one from a capping water molecule, and one oxygen atom from a carboxylate group on a second ligand in the tetramer, see Figure 4. The tetramers enclose the hydrophilic surface of the complexes, and expose the hydrophobic surface of the cyclen ring, creating hydrophobic pores in the structure. In the crystal structure the coumarin units exhibit π-π stacking. The overall structure of the complex is the square antiprismatic form **SAP** expected for a DO3A complex, and in the crystal the **Eu**.**L** is in the open form (contrasts Figures 2 and 4).

Solution structure part I

The solution structure alluded to in Figure 2 must be considered when inspecting the ^{1}H NMR spectra in Figure 3. The diamagnetic species **Y**.**L** and H_3.**L** show sharp resonances from protons on the coumarin and carboxylate arms. The ring protons can be identified in the free ligand, while those in the yttrium complex give rise to overlapping and broad signals implying exchange between multiple closely related species. The paramagnetic ^{1}H NMR spectrum of the **Eu**.**L** and **Tb**.**L** complexes give rise to resonances in a wide ppm region. The paramagnetic ^{1}H NMR spectra of Ln.DO3A and Ln.DOTA complexes are well understood.[61-66] Tb^{3+} complexes with functionalised DO3A ligands usually give rise to four resonances arising from the axial protons of the cyclen ring between -350 and -400 ppm for the square anti-prismatic **SAP** conformation of the complex. Similarly, the axial protons of Eu^{3+} complexes derived from DO3A give rise to four resonances around 40 ppm. For the europium(III) complex both the **SAP** and the twisted square anti-prismatic **TSAP** conformation must be considered. The latter gives rise to resonances from the axial protons around 20 ppm. Figure 3 shows that the spectra of **Eu**.**L** and **Tb**.**L** do not show four distinct resonances of the axial cyclen protons. Rather a single resonance is observed at a significantly lower ppm than was expected for an axial proton in the **SAP** conformation of DO3A. This indicates that the structure of the complexes is in rapid exchange between several diastereoisomers on the NMR timescale. Exchange between **SAP** and **TSAP** should not make the resonances from different axial protons coalesce. At this point we speculate the equilibrium between an open and closed form as proposed in Figure 2 is the cause of this observation. Note that the signal from the **SAP** form is observed as a single resonance for both **Eu.L** and **Tb.L**. We have previously attributed this form of spectrum to complexes of flexible DO3A ligands that is ligands without a fourth coordinating pendant arm.[67] The acetate resonances between 280-200 ppm are clearly resolved the **Tb**.**L** spectrum. This indicates that an open form does not contribute significantly to the solution structure of this complex.

Lanthanide centred luminescence

The **Eu**.**L** and **Tb**.**L** complexes luminesce following excitation of the lanthanide centre or the coumarin chromophore. In the excitation spectra of the complexes (Figure 5 and ESI), the absorption bands corresponding to direct excitation of the lanthanide ions cannot be distinguished, indicating that the lanthanide excited state are predominantly populated through excitation of the coumarin chromophore. As we reported recently,[55] the coumarin chromophore is an efficient sensitiser for europium(III), while only very weak terbium(III) centred luminescence could be observed. This is unexpected as the energy level of the coumarin-centred excited state should be able to populate the lanthanide centred excited states.[38] We must conclude that all terbium(III) centred emission arises from energy transfer from the antenna singlet state, *vide infra*. By inspection of Figure 6 it can be seen that direct energy transfer to the europium(III) excited state manifold is possible to e.g. the $^5G_4$ and $^5L_6$ states, however, in the terbium(III) excited state manifold the $^5D_3$ state lies below the S_1 state but is above the T_1 state of the antenna chromophore. This suggests that excited state energy transfer via a Dexter exchange mechanism favours energy transfer through the intermediate states in the excited state manifold.[57]

If efficient energy transfer was possible from T_1 to the terbium(III) centre, a quantum yield of luminescence ϕ_{HEPES} for terbium(III) should be higher than that for europium(III). We can speculate that the energy difference between the antenna centred triplet state and lanthanide centred excited state is too large to allow for efficient energy transfer to occur,[57, 58] see Figure 6. This is in direct conflict with previously published results.[38]

Table 1 shows the luminescent properties of the **Eu**.**L** and **Tb**.**L** complexes. By determining the luminescence lifetimes and using the modified Horrocks' equation, the number of solvent molecules coordinated to the lanthanide centre *q* was determined.[68, 69] For **Eu**.**L** *q* = 2 and for **Tb**.**L** *q* = 1 confirming the difference observed in the ^{1}H NMR spectra, see figure 3. The difference was further confirmed by the stability constants of the two complexes.[55] Despite the similarities of the two ions, see Figure 1, the europium(III) complex is 2 orders of magnitude less stable than the terbium(III) complex. Clearly, the solution structure of the two complexes differs, which in turn must influence the photophysical properties of the complexes as indicated in Figure 2.

Table 1. Luminescence properties of **Eu**.**L** and **Tb**.**L** complexes in 0.1 M HEPES buffer at pH 7.4, all data can be seen in the ESI.

	Eu.**L**	**Tb**.**L**[a]
τ_{H2O} (ms)	0.41	0.93
τ_{D2O} (ms)	1.63	1.24
q[b]	1.90	0.96
Ln ϕ_{HEPES} (%)	5.26	-
Logβ[c]	26.92 ± 0.2	28.71 ± 0.1

[a] Lifetimes were determined in aerated and degassed samples and were unchanged. [b] equations $q = A(\tau_{H2O}^{-1} - \tau_{D2O}^{-1} - B)$, for europium(III) A = 1.2 ms and B = 0.25 ms, for terbium(III) A = 5.0 ms and B = 0.06 ms .[68, 70] [c] from reference [55].

Antenna centred fluorescence

The paramagnetic ^{1}H NMR and the lanthanide centred luminescence show that at least two conformers are present in solution and that the speciation in **Eu**.**L** and **Tb**.**L** differs. Figure 5 shows the excitation and emission spectra of **Eu**.**L**, and H_3.**L**. Apart from the additional europium(III) centred bands in the emission spectrum, Figure 5 shows that in steady-state conditions the ligand centred optical transition is unchanged by protonation state and complexation of a trivalent metal ion. Figure 5 includes the phosphorescence spectrum recorded at 77 K, which enables the determination of the energy of the coumarin-centred triplet excited state T_1. Figure 6 shows the energy levels of the first singlet S_1 and triplet T_1 excited state in the coumarin chromophore along the lowest energy levels of Eu^{3+}, Gd^{3+}, and Tb^{3+} ions. Cursory inspection of Figure 6 shows the excited state energy transfer from S_1 can occur to the $^5D_3$ state of Tb^{3+} and to several states in the excited state manifold of Eu^{3+}. Excited state energy transfer from T_1 to the Tb^{3+} excited

state manifold does not seem feasible as there are no states of similar energy. For Eu^{3+}, the $^5L_6$ and $^5D_3$ states are of similar energy to the T_1 state, which allow excited state energy transfer to be possible. The *f-f* transitions of Gd^{3+} are not accessible in energy, and neither are the excited states of Y^{3+} ion, the latter is not included in Figure 6.

All lanthanide centred emission in this system originates from the first singlet excited state of the coumarin. Therefore, a detailed understanding of the excited state processes depopulating the S_1 state in the **Y**.**L**, **Eu**.**L**, **Gd**.**L**, **Tb**.**L**, H_3.**L**, and H_5.$\mathbf{L}^{2+}$ are required.

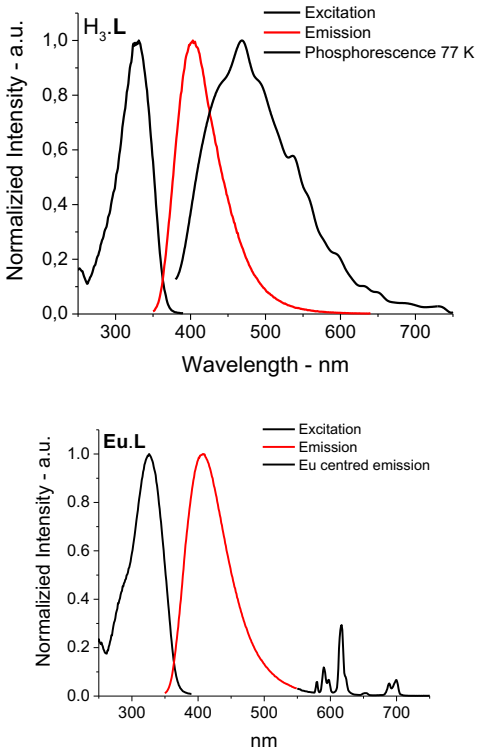

Figure 5. Excitation and emission spectra of H_3**L** (top) and **Eu.L** (bottom). Both excitation spectra followed emission at 402 nm. Emission spectra followed excitation at 325 nm measured at room temperature in HEPES buffer at pH 7.4 The phosphorescence spectrum of H_3**L** was recorded at 77 K. Data for all complexes can be seen in the ESI.

Figure 6 includes arrows corresponding to the processes that depopulate S_1 in the absence of a lanthanide ion: Fluorescence k_f, non-radiative deactivation via internal conversion to S_0 k_{ic}, and intersystem crossing to T_1 k_{isc}. In Table 2 each process is listed with the first order rate constant of the process. The total non-radiative decay from S_1 is $k_{nr} = k_{ic} + k_{isc}$. In presence of a lanthanide ion, or other quenchers, additional pathways of deactivation become possible. These processes are listed in Figure 2. All paramagnetic lanthanide ions add induced intersystem crossing $k_{isc'}$ as a deactivation pathway for S_1. This is a medium effect and comes into effect above a critical concentration of lanthanide ions in solution.[56] Two other deactivation pathways are possible: photoinduced electron transfer k_{PeT} if a lanthanide ion with suitable redox chemistry is complexed, and excited state energy transfer k_{EnT} if a lanthanide ion with a close lying excited state is coordinated. These processes are both distance dependent.[57, 58] PeT and energy transfer via the Dexter mechanism requires that the chromophore and lanthanide ion collide, resulting in orbital overlap. Therefore, the magnitude of k_{PeT} and k_{EnT} will be directly linked to the solution structure of the complex, see Figure 2.

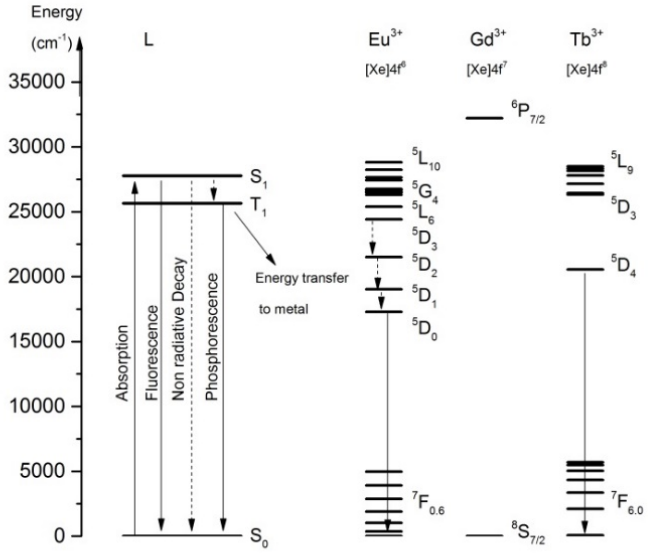

Figure 6. Energy levels of the coumarin antenna chromophore (**L**) and the Eu^{3+}, Gd^{3+}, and Tb^{3+}, free ions.

The photophysical properties of **Y**.**L**, **Eu**.**L**, **Gd**.**L**, **Tb**.**L**, and H_3.**L** are compiled in Table 2. The energies of states in the coumarin excited state manifold is not changed by the trivalent lanthanide ions, but the fluorescence quantum yield $\phi_{F(H2O)}$ is significantly reduced in the europium(III) complex. This is to be expected as Eu^{3+} is an efficient PeT quencher.[71-73] More surprising is the fact Tb^{3+} also reduces the fluorescence quantum yield, as this can only occur by energy transfer to the terbium(III) centre. This is confirmed by the data from the Gd^{3+} and Y^{3+} complexes. For **Y**.**L** the fluorescence quantum yield is increased. This is due to the coordination of the cyclen nitrogen atoms that in H_3.**L** gives rise to PeT quenching.

By determining the amplitude averaged excited state lifetime of S_1 $\langle\tau\rangle$, the rate constant for depopulation S_1 k_{obs} can be determined. From $\langle\tau\rangle$ and ϕ_F the k_{obs} can be separated into radiative k_f and a non-radiative k_{nr} contribution. Table 2 includes these numbers for all complexes.

By comparing the five compounds, we can go a step further. **Y**.**L** does not allow for induced intersystem crossing, excited state energy transfer, and photoinduced electron transfer quenching. **Gd**.**L** contributes only to induced intersystem crossing, while for **Tb**.**L** excited state energy transfer may be possible. **Eu**.**L** may have induced intersystem crossing, excited state energy transfer, and photoinduced electron transfer quenching. Finally, H_3.**L** will only show photoinduced electron transfer quenching by the aza bridged cyclen. These stipulations allow the rate

constants for the individual processes to be separated as done in Table 2. The most noteworthy entry in Table 2, is that excited state energy transfer from S_1 to the terbium(III) excited state manifold occurs with a rate constant equal to k_f. It follows directly that the quantum yield of energy transfer ϕ_{EnT} must be equal to the quantum yield of fluorescence: $\phi_F = \phi_{EnT} = 18$ %, which should, but does not, give rise to a significant amount of terbium(III) centred luminescence. Thus back energy transfer from the terbium(III) centre to the antenna chromophore T_1 state must be possible. The numbers in Table 2 also show that induced intersystem crossing does not influence the depopulation of S_1 to an appreciable degree. Note that k_{EnT} and k_{PeT} cannot be separated for the europium(III) complex.

Table 2. Photophysical properties of H_3.**L**, **Eu**.**L**, **Gd**.**L**, and **Tb**.**L**. The data and fits leading to the reported values are available as ESI.

	H_3.**L**	**Eu**.**L**	**Gd**.**L**	**Tb**.**L**	**Y**.**L**
λ_{abs} (nm)	328	326	327	328	329
ε (M^{-1} cm^{-1})	7454	3287	3405	3601	3859
logε ($M^{-1}cm^{-1}$)	3.87	3.52	3.53	3.56	3.59
E_T (cm^{-1})	26,042	25,000	25,000	25,000	25,000
E_{Ln} (cm^{-1})					
$\phi_{F(H2O)}$ (%)	20	7.3	21	18	24
$<\tau_{F(H2O)}>$ (ns)	0.81	0.53	1.7	1.3	1.7
$<\tau_{F(D2O)}>$ (ns)	0.86	0.96	1.6	1.7	1.8
τ_0 (ns) [a]	4.0	7.3	8.2	7.5	7.2
k_f (10^8 s^{-1}) [b]	2.5	1.4	1.2	1.3	1.4
k_{obs} (10^8 s^{-1}) [c]	12	19	5.9	7.5	5.9
k_{nr} (10^8 s^{-1}) [d]	9.8	18	4.6	6.1	4.5
k_{PeT} (10^8 s^{-1}) [e]	5.3	13	-	-	-
k_{EnT} (10^8 s^{-1}) [f]	-		-	1.6	-

[a] $\tau_0 = \tau_{F(H2O)}/\ \phi_{F(H2O)}$. [b] $k_{obs} = 1/\tau_{F(H2O)}$. [c] $k_f = 1/\tau_0$. [d] $k_{nr} = k_{obs} - k_f$. [e] for H_3.**L**: $k_{PeT} = k_{nr} - k_{nr}$(Y/Gd). [f] for **Tb**.**L**: $k_{EnT} = k_{nr} - k_{nr}$(Y/Gd).

Solution Structure part II

The values reported in Table 2 are averages. The quantum yield of fluorescence $\phi_{F(H2O)}$ is a weighted average of contributions from all possible emitting species in solution. And in Table 2 the amplitude averaged fluorescence lifetime $<\tau_{F(H2O)}>$ is used. While the number of emitting species cannot be resolved in the steady-state experiments, the time-resolved data provides this information, and shows the contribution from two different emitting species. Thus the antenna chromophore photophysics show that two conformations are present in solution. With support from the ^{1}H NMR, the stability constants logβ, and the number of solvent molecules bound at the lanthanide centre q we can draw up the equilibrium shown in figure 7. Figure 7 also includes a molecular model that shows the two isomers, where the coumarin is either in contact with the metal centre or as far as possible from the metal centre. The latter is similar to the crystal structure found for **Eu**.**L**.

The difference in the distance between the antenna chromophore and the metal centre should influence the photophysics of the antenna chromophore as outlined in Figure 2. Indeed, the time resolved data showed two emitting species, one with a ca. 2 ns S_1 lifetime and one where the S_1 lifetime is ca. 0.6 ns. To elucidate which species corresponds to the open and closed confirmations (Figures 2 and 7), time-resolved emission spectra were recorded. Two forms of the free ligand were included, as the amino groups of the cyclen ring are efficient PeT quenchers. Quenchers can be removed by protonation, which allows us to determine the photophysical properties of the antenna chromophore with and without additional pathways for deactivation of S_1. The results are compiled in Table 3.

In the time-resolved emission spectra, three emission bands with distinct excited state lifetimes (τ_1, τ_2, and τ_3) were resolved, two bands (τ_2, and τ_3) with identical shape and emission maxima corresponding to the antenna chromophore fluorescence. The third band τ_1, a minor contribution, is a red-shifted band that coincides with coumarin phosphorescence. The phosphorescence lifetime is reduced to nanoseconds due to quenching by oxygen, but is clearly resolved on the red side of the fluorescence, see the ESI. τ_1 is not seen in **Gd**.**L**, which may be due to rapid induced intersystem crossing from T_1 to S_1.[56]

Two conformations (τ_2, and τ_3) are differentiated in the time-resolved emission spectra. The distribution between τ_2, and τ_3 vary within the series of compounds **Y**.**L**, **Eu**.**L**, **Gd**.**L**, **Tb**.**L**, H_3.**L**, and H_5.**L**$^{2+}$ but fall in two groups. **Y**.**L**, **Gd**.**L**, and **Tb**.**L** are primarily (≥80%) in the conformation with the long fluorescence lifetime τ_2. In contrast, **Eu**.**L**, H_3.**L**, and H_5.**L**$^{2+}$ are primarily found in the other (>60%) conformation characterised by the shorter τ_3 lifetime. Clearly, **Eu**.**L** has a different solution structure than **Y**.**L**, **Gd**.**L**, **Tb**.**L**. Note that the time-resolved emission spectrum following the antenna chromophore fluorescence can reveal the solution structure as the nanosecond timescale is faster than the conformational fluctuations. The lanthanide luminescence does not reveal conformational fluctuations, as the millisecond luminescence lifetime will only report the weighted average. In this case, the difference between the two conformers and the ratio 20:80 vs 80:20 are large enough to be seen in q.

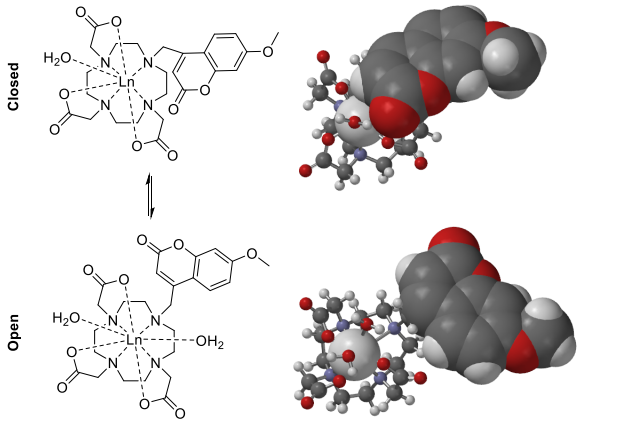

Figure 7. Equilibrium of the molecular solution state structure of the complexes. Ln = Y(III), Eu(III), Gd(III) and Tb(III), and a molecular model of the structure (right).

In Figure 2 two conformations were labelled open and closed, and Table 3 includes two conformations τ_2, and τ_3. In the free

ligand, photoinduced electron transfer quenching requires direct contact between the coumarin chromophore and the cyclen nitrogen atoms. PeT is only possible in H_3.**L** as the amino groups are protonated in H_5.$\mathbf{L}^{2+}$ and cannot act as PeT quenchers. Table 3 shows that τ_3 is very similar in the two compounds, indicating that a lifetime of 0.5-0.6 ns corresponds to the lifetime of the antenna chromophore in the open form. Water must be an efficient quencher for the coumarin S_1 state. In H_3.**L**, PeT quenching reduces the τ_2 lifetime by 0.8 ns compared to H_5.$\mathbf{L}^{2+}$ confirming that τ_2 corresponds to the closed conformation. Thus, the solution structure of **Eu**.**L** is the open conformation in complete agreement with the results presented above. Both the open (τ_3 = 0.3 ns) and the closed (τ_2 = 1.3 ns) conformer of **Eu**.**L** have a shorter lifetime than the free ligand, which matches the lower fluorescence quantum yield determined for **Eu**.**L**.

Y.**L**, **Gd**.**L**, and H_5.$\mathbf{L}^{2+}$ has a lifetime of τ_2 = 2 ns and τ_3 = 0.4-0.8 ns in the closed and open conformer, respectively. The reduced lifetime of the closed conformation of **Tb**.**L** (τ_2 = 1.5 ns) confirms that the chromophore S_1 state must be depopulated by excited state energy transfer to terbium(III). The inefficient population of the emitting $^5D_4$ state of Tb^{3+} must be due to back energy transfer to the chromophore T_1 state.

Table 3. Fluorescence lifetime τ and fractional amplitude A determined from a global fit of time-resolved emission spectra of **Y**.**L**, **Eu**.**L**, **Gd**.**L**, **Tb**.**L**, H_3.**L**, and H_5.$\mathbf{L}^{2+}$ in HEPES buffer at pH 7.4, data and fits can be found as ESI.

H_2O	H_5.$\mathbf{L}^{2+}$	H_3.**L**	Eu.L	Gd.L	Tb.L	Y.L
τ_1[a] (ns)	-	3.5	2.9	-	2.9	3.6
A_1 (%)	0	1	4	0	2	2
τ_2[a] (ns)	2.1	1.3	1.3	2.0	1.5	1.9
A_2 (%)	35	28	15	80	81	82
τ_3[a] (ns)	0.6	0.5	0.3	0.8	0.4	0.4
A_3 (%)	65	71	81	20	17	16

[a] error < 0.1 ns, see ESI for details.

Conclusion

Rationalising the photophysical and physicochemical properties of lanthanide dyes exploiting the antenna effect is still a work in progress. By synthesising lanthanide complexes of a 4-methyl-7-methoxy-coumarin appended 1,4,7,10-tetraazadodecane-1,4,7-triacetic acid (DO3A) ligand we are able to conclude that detailed studies of solution structure and residual sensitiser fluorescence is essential if we are to complete the work.

Our detailed investigation exploiting ^{1}H NMR, europium(III) and terbium(III) centred luminescence, model systems, and detailed fluorescence spectroscopy allows us to conclude: i) that the **Ln**.**L** system exists in two conformations in solution. ii) that the europium(III) and terbium(III) complex are significantly different, much more than the small difference in ionic radius dictates. iii) that excited state energy transfer from short lived ($\langle\tau_F\rangle \approx 2$ ns) excited states to lanthanide centred states can occur with high efficiencies. And iv) that back energy transfer from the lanthanide centre to lower lying ligand centred excited state can occur with high efficiency.

Experimental

Materials and methods

All chemicals for synthesis were used as received. All solvents for spectroscopic experiments were of HPLC grade and used as received. Water was deionized and microfiltered using a Milli-Q Millipore machine. Chromatographic purification was performed on silica gel (SiO2) with pore size of 60 Å and particle size of 60–200 µm. Mass spectra were recorded on a high resolution Micro-TOF-QII-system using ESP (calibrated using formic acid). ^{1}H NMR spectra were recorded on a Brucker 500 MHz instrument. ^{13}C NMR spectra were recorded on a Bruker 126 MHz instrument equipped with a (noninverse) cryoprobe. All chemical shifts (δ) are given in parts per million.

Synthetic procedures

1-(7-methoxy-4-methyl-coumarin)-4-7-10--tris(tert-butoxycarbonylmethyl)-1,4,7,10-tetraazacyclododacane (1). 4-Bromomethyl-7-methoxy-coumarin (546.7 mg, 2.03 mmol) was dissolved in acetonitrile (30 ml) together with 1,4,7-Tris(tert-butylcarbonylmethyl)-1,4,7,10-tetracyclododacane (1.10 g, 1.85 mmol) and potassium carbonate (1.15 g, 8.31 mmol), the mixture was heated to 60°C and stirred overnight. After the reaction was complete the mixture was filtered and washed with dichloromethane. The filtrate was then evaporated to dryness under reduced vacuum. The crude product was purified by column chromatography (10 % MeOH/DCM). Yield 586 mg, 45%. ESI-MS: m/z calculated for $C_{37}H_{58}N_4O_9$ $[M+H]^+$ 703.4276, found 703.4287. ^{1}H NMR (500 MHz, Chloroform-*d*) δ 7.67 (d, *J* = 8.9 Hz, 1H), 6.85 (dd, *J* = 8.8, 2.6 Hz, 1H), 6.82 (d, *J* = 2.5 Hz, 1H), 6.45 (s, 1H), 4.12 (s, 2H), 3.87 (s, 5H), 3.57 (s, 3H), 3.31 (s, 3H), 3.19 (s, 7H), 3.00 (d, *J* = 5.3 Hz, 4H), 1.49 (s, 9H), 1.40 (s, 18H). ^{13}C NMR (126 MHz, $CDCl_3$) δ 173.69, 172.79, 163.03, 160.59, 155.62, 152.54, 125.59, 112.81, 112.59, 111.79, 101.49, 101.21, 83.33, 82.62, 56.74, 55.92, 55.85, 55.33, 54.46, 51.76, 51.40, 28.38, 28.34, 28.22, 28.19, 28.10, 28.03.

1-(7-methoxy-4-methyl-coumarin)-4-7-10-tris(carboxylmethyl)-1,4,7,10-tetraazacyclododacane (L). Proligand **1** (586 mg, 0.83 mmol) was dissolved in dichloromethane (10 ml), trifluoroacetic acid (10 ml) was then added to the mixture. The reaction mixture was left to stir for 48 hours at room temperature. The solvent was removed under reduced pressure and the residue dissolved in the minimum amount of methanol and precipitated with diethyl ether. Trituration with diethyl ether yielded the product as a slightly yellow solid in quantitative yield. ESI-MS: m/z calculated for $C_{25}H_{34}N_4O_9$ $[M+H]^+$ 535.2398, found 535.2398. ^{1}H NMR (500 MHz, Deuterium Oxide) δ 7.93 (d, *J* = 8.8 Hz, 1H), 7.05 – 6.98 (m, 2H), 6.65 (s, 1H), 4.12 (s, 2H), 3.94 – 3.91 (m, 3H), 3.86 (d, *J* = 16.8 Hz, 2H), 3.64 – 3.36 (m, 13H), 3.09 (dd, *J* = 58.6, 28.0 Hz, 10H).

General method for the complexes Ln.L.

To a solution of the ligand (H_3.**L**) in methanol the appropriate lanthanide triflate salt was added (1.1 eq.) and the reaction mixture was stirred at 60 °C for 30 min. at which point the pH of the solution was adjusted to ~ 4 by dropwise addition of hydrochloric acid (2 M). The reaction was left stirring at 60 °C

for 48 h. The methanol was removed under reduced pressure leaving an oil that was dissolved in water. The pH was adjusted to ~ 10 by addition of sodium hydroxide (1M) to remove excess lanthanide as its insoluble hydroxide. The resulting precipitate was centrifuged and the supernatant filtered through a syringe filter. The solvent was removed under reduced pressure to obtain the product as an off-white solid.

Eu.L: Yield 85 %. ESI-MS: m/z calculated for $C_{25}H_{31}EuN_4O_9$ $[M+Na]^+$ 707.1198, found 707.1201. ^1H NMR (500 MHz, D_2O) δ 33.86, 24.40, 13.10, 12.40, 11.47, 10.00, 9.52, 8.19, 7.72, 6.97, 6.94, 6.22, 3.84, 3.27, 2.75, 1.24, 1.18, 0.78, 0.04, -1.11, -4.67, -5.81, -7.29, -9.31, -10.13, -11.68, -12.54, -13.15, -13.49, -13.70, -15.25, -18.38.

Tb.L: Yield 93 %. ESI-MS: m/z calculated for $C_{25}H_{31}N_4O_9Tb$ $[M+H]^+$ 691.1417, found 691.1440. ^1H NMR (500 MHz, D_2O) δ 261.53, 241.73, 231.34, 210.21, 162.77, 150.61, 113.56, 103.02, 95.94, 81.98, 68.59, 57.62, -21.15, -26.60, -28.65, -34.72, -37.37, -41.41, -48.78, -55.54, -57.04, -59.69, -63.83, -77.43, -80.43, -98.17, -104.35, -107.63, -122.12, -139.75, -145.22, -149.28, -169.10, -184.57, -205.02, -215.04, -225.90, -296.13. Only resolved peaks outside the -40 – 40 ppm region are reported.

Gd.L: Yield 82 %. ESI-MS: m/z calculated for $C_{25}H_{31}GdN_4O_9$ $[M+H]^+$ 690.1411, found 690.1491.

Y.L: Yield 86 %. ESI-MS: m/z calculated for $C_{25}H_{31}YN_4O_9$ $[M+H_3O^+]^+$ 639.1327, found 639.1348. ^1H NMR (500 MHz, Deuterium Oxide) δ 6.89 (m, 1H), 6.19 (m, 3H), 5.93 (dd, *J* = 5.8, 2.8 Hz, 1H), 3.85 – 3.78 (m, 4H), 3.29 – 2.90 (m, 10H), 2.79 – 2.24 (m, 30H).

Optical Spectroscopy

Absorption spectra were measured with a Cary 300 UV-Vis double beam spectrometer from Agilent Technologies against air using pure solvent as baseline. The fluorescence and time-gated emission spectra were recorded on a Cary Eclipse fluorescence spectrometer with a photomultiplier tube from Agilent Technologies. The fluorescence and metal centred lifetimes were determined using a FluoTime 300 instrument from PicoQuant. The excitation source was the 355 nm line from a VisUV laser or a Xenon Cw lamp from PicoQuant. The data was fitted as monoexponential or triexponential decay using the deconvolution as implemented in the FluoFit software (version 4.6.6) from PicoQuant. The phosphorescence measurements were done on a Cary Eclipse fluorescence spectrometer with a photomultiplier tube from Agilent Technologies

For all spectroscopic measurements, the absorbance at the excitation wavelength was kept below 0.1 to avoid inner filter effects and intermolecular interactions. Absorption and fluorescence experiments at ambient temperatures were performed in 10.00 mm Hellma quartz fluorescence cuvettes. The phosphorescence experiments at 77 K were performed in Dewar fitted with a quartz cold finger accessory; the sample solution was placed in a quartz tube, positioned in the Dewar and flash frozen using liquid nitrogen.

Quantum yields were determined against quinine sulphate in 0.1 N sulphoric acid, see supporting information for details.

Crystallography

Multiple attempts were made to determine the structure of **Eu.L** using low temperature single crystal X-ray diffraction. Data were variously collected using a (Rigaku) Oxford Diffraction Supernova, an XtaLAB Synergy with HyPix detector and synchrotron radiation using I19-1 at Diamond Light Source.[74] Data were reduced using CrysAlisPro or Xia2[75] as appropriate and solved using ShelXT[76] or Superflip[77] prior to refinement with CRYSTALS[78,79,80]. In each case, the voids were tre3ated using PLATON/SQUEEZE.[81, 82] Three polymorphs/solvates were found all exhibiting the same tetrameric packing. Further details can be found in the ESI; crystallographic data in CIF format are also available and have been deposited with the Cambridge Crystallographic Data Centre (CCDC XXXX-XXXX).

Conflicts of interest

There are no conflicts to declare.

Acknowledgements

The authors thank Oticon Fonden, Diamond Light Source for an award of beamtime (MT13639), Carlsbergfondet, Knud Højgaards Fond, Villum Fonden (grant#14922), Kirsten E. Christensen for support, Cancer Research UK, Cancer Imaging Centre Oxford, the University of Copenhagen, and Dyanne Cruickshank and Rigaku Oxford Diffraction for help with collection of diffraction data using the XtaLAB Synergy.

Notes and references

1. P. Hänninen and H. Härmä, *Lanthanide Luminescence*, Springer, Heidelberg, 2011.
2. A. de Bettencourt-Dias, *Luminescence of Lanthanide Ions in Coordination Compounds and Nanomaterials*, John Wiley & Sons Ltd, 2014.
3. J. C. G. Bunzli, *Coordination Chemistry Reviews*, 2015, **293**, 19-47.
4. W. T. Carnall, in *Handbook on the Physics and Chemistry of Rare Earths*, eds. Karl A. Gschneidner, Jr. and E. LeRoy, Elsevier, 1979, vol. Volume 3, pp. 171-208.
5. R. P. Haugland, *Handbook of Fluorescent Probes and Research Chemicals*, Molecular Probes, Eugene, Oregon, 11th edn., 2010.
6. L. D. Lavis and R. T. Raines, *ACS Chem. Bio.*, 2008, **3**, 142-155.
7. A. T. Frawley, R. Pal and D. Parker, *Chem Commun (Camb)*, 2016, **52**, 13349-13352.
8. J. M. Zwier and N. Hildebrandt, in *Reviews in Fluorescence 2016*, ed. C. D. Geddes, Springer, 2017, DOI: 10.1007/978-3-319-48260-6_3, pp. 17-43.
9. D. Geißler, S. Stufler, H.-G. Löhmannsröben and N. Hildebrandt, *Journal of the American Chemical Society*, 2012, **135**, 1102-1109.
10. M. Delbianco, V. Sadovnikova, E. Bourrier, G. Mathis, L. Lamarque, J. M. Zwier and D. Parker, *Angewandte Chemie*, 2014, **53**, 10718-10722.
11. A. T. Bui, A. Grichine, A. Duperray, P. Lidon, F. Riobe, C. Andraud and O. Maury, *Journal of the American Chemical Society*, 2017, **139**, 7693-7696.

12. Z. Liao, M. Tropiano, K. Mantulnikovs, S. Faulkner, T. Vosch and T. Just Sørensen, *Chemical Communications*, 2015, **51**, 2372-2375.
13. Z. Liao, M. Tropiano, S. Faulkner, T. Vosch and T. J. Sørensen, *RSC Adv.*, 2015, DOI: 10.1039/c5ra15759e, 70282–70286.
14. H. Siitari, I. Hemmilä, E. Soini, T. Lövgren and V. Koistinen, *Nature*, 1983, **301**, 258-260.
15. I. Hemmilä, S. Dakubu, V.-M. Mukkala, H. Siitari and T. Lövgren, *Analytical Biochemistry*, 1984, **137**, 335-343.
16. G. Marriott, R. M. Clegg, D. J. Arndt-Jovin and T. M. Jovin, *Biophys J*, 1991, **60**, 1374-1387.
17. P. R. Selvin, *Annu Rev Biophys Biomol Struct*, 2002, **31**, 275-302.
18. G. Vereb, E. Jares-Erijman, P. R. Selvin and T. M. Jovin, *Biophys J*, 1998, **74**, 2210-2222.
19. J.-C. G. Bünzli, in *Luminescence of Lanthanide Ions in Coordination Compounds and Nanomaterials*, John Wiley & Sons Ltd, 2014, DOI: 10.1002/9781118682760.ch04, pp. 125-196.
20. F. S. Richardson, *Chemical Reviews*, 1982, **82**, 541-552.
21. M. C. Heffern, L. M. Matosziuk and T. J. Meade, *Chem Rev*, 2014, **114**, 4496-4539.
22. A. Grichine, A. Haefele, S. Pascal, A. Duperray, R. Michel, C. Andraudd and O. Maury, *Chem. Sci.*, 2014, **5**, 3475.
23. E. G. Moore, A. P. Samuel and K. N. Raymond, *Acc Chem Res*, 2009, **42**, 542-552.
24. W. S. Perry, S. J. Pope, C. Allain, B. J. Coe, A. M. Kenwright and S. Faulkner, *Dalton transactions*, 2010, **39**, 10974-10983.
25. H. Uh and S. Petoud, *Comptes Rendus Chimie*, 2010, **13**, 668-680.
26. E. Pershagen, J. Nordholm and K. E. Borbas, *Journal of the American Chemical Society*, 2012, **134**, 9832-9835.
27. L. Armelao, S. Quici, F. Barigelletti, G. Accorsi, G. Bottaro, M. Cavazzini and E. Tondello, *Coordination Chemistry Reviews*, 2010, **254**, 487-505.
28. S. Faulkner, L. S. Natrajan, W. S. Perry and D. Sykes, *Dalton transactions*, 2009, DOI: 10.1039/b902006c, 3890-3899.
29. A. D'Aleo, E. G. Moore, J. Xu, L. J. Daumann and K. N. Raymond, *Inorganic chemistry*, 2015, **54**, 6807-6820.
30. P. Kadjane, L. Charbonniere, F. Camerel, P. P. Laine and R. Ziessel, *Journal of fluorescence*, 2008, **18**, 119-129.
31. F. Kielar, G. L. Law, E. J. New and D. Parker, *Organic & biomolecular chemistry*, 2008, **6**, 2256-2258.
32. J. F. Lemonnier, L. Guenee, C. Beuchat, T. A. Wesolowski, P. Mukherjee, D. H. Waldeck, K. A. Gogick, S. Petoud and C. Piguet, *Journal of the American Chemical Society*, 2011, **133**, 16219-16234.
33. M. Soulie, F. Latzko, E. Bourrier, V. Placide, S. J. Butler, R. Pal, J. W. Walton, P. L. Baldeck, B. Le Guennic, C. Andraud, J. M. Zwier, L. Lamarque, D. Parker and O. Maury, *Chem Eur J*, 2014, **20**, 8636-8646.
34. E. Kasprzycka, V. A. Trush, V. M. Amirkhanov, L. Jerzykiewicz, O. L. Malta, J. Legendziewicz and P. Gawryszewska, *Chemistry*, 2017, **23**, 1318-1330.
35. T. Lazarides, M. A. Alamiry, H. Adams, S. J. Pope, S. Faulkner, J. A. Weinstein and M. D. Ward, *Dalton transactions*, 2007, DOI: 10.1039/b700714k, 1484-1491.
36. A. Beeby, S. Faulkner, D. Parker and J. A. G. Williams, *Journal of the Chemical Society, Perkin Transactions 2*, 2001, DOI: 10.1039/b009624p, 1268-1273.
37. A. Dadabhoy, S. Faulkner and P. G. Sammes, *Journal of the Chemical Society, Perkin Transactions 2*, 2000, DOI: 10.1039/b008179p, 2359-2360.
38. M. Latva, H. Takalo, V.-M. Mukkala, C. Matachescu, J. C. Rodriguez-Ubis and J. Kankare, *Journal of Luminescence*, 1997, **75**, 149-169.
39. J. D. Routledge, M. W. Jones, S. Faulkner and M. Tropiano, *Inorganic chemistry*, 2015, **54**, 3337-3345.
40. B. Alpha, R. Ballardini, V. Balzani, J. M. Lehn, S. Perathoner and N. Sabbatini, *Photochem Photobiol*, 1990, **52**, 299-306.
41. C. Szijjarto, E. Pershagen, N. O. Ilchenko and K. E. Borbas, *Chem Eur J*, 2013, **19**, 3099-3109.
42. H. Sund, K. Blomberg, N. Meltola and H. Takalo, *Molecules*, 2017, **22**.
43. A. D'Aleo, G. Pompidor, B. Elena, J. Vicat, P. L. Baldeck, L. Toupet, R. Kahn, C. Andraud and O. Maury, *Chemphyschem : a European journal of chemical physics and physical chemistry*, 2007, **8**, 2125-2132.
44. A. Picot, A. D'Aléo, P. L. Baldeck, A. Grichine, A. Duperray, C. Andraud and O. Maury, *Journal of the American Chemical Society*, 2008, **130**, 1532-1533.
45. A. D'Aléo, C. Andraud and O. Maury, in *Luminescence of Lanthanide Ions in Coordination Compounds and Nanomaterials*, John Wiley & Sons Ltd, 2014, DOI: 10.1002/9781118682760.ch05, pp. 197-230.
46. D. Lundberg and I. Persson, *Coordination Chemistry Reviews*, 2016, **318**, 131-134.
47. I. Hemmilá and V.-M. Mukkala, *Critical Reviews in Clinical Laboratory Sciences*, 2008, **38**, 441-519.
48. T. Lazarides, D. Sykes, S. Faulkner, A. Barbieri and M. D. Ward, *Chemistry*, 2008, **14**, 9389-9399.
49. M. Tropiano, O. A. Blackburn, J. A. Tilney, L. R. Hill, M. P. Placidi, R. J. Aarons, D. Sykes, M. W. Jones, A. M. Kenwright, J. S. Snaith, T. J. Sørensen and S. Faulkner, *Chem Eur J*, 2013, **19**, 16566-16571.
50. T. J. Sørensen, M. Tropiano, A. M. Kenwright and S. Faulkner, *European Journal of Inorganic Chemistry*, 2017, **2017**, 2165-2172.
51. T. J. Sørensen, A. M. Kenwright and S. Faulkner, *Chemical Science*, 2015, **6**, 2054-2059.
52. D. Kovacs, X. Lu, L. S. Meszaros, M. Ott, J. Andres and K. E. Borbas, *Journal of the American Chemical Society*, 2017, **139**, 5756-5767.
53. J. Andres and K. E. Borbas, *Inorganic chemistry*, 2015, **54**, 8174-8176.
54. C. Szijjarto, E. Pershagen and K. E. Borbas, *Dalton transactions*, 2012, **41**, 7660-7669.
55. A. K. R. Junker, G. J. Deblonde, R. J. Abergel and T. J. Sørensen, manuscript submitted.
56. R. Arppe, N. Kofod, A. K. R. Junker, L. G. Nielsen, E. Dallerba and T. Just Sørensen, *European Journal of Inorganic Chemistry*, 2017, **2017**, 5246-5253.
57. B. Valeur, *Molecular Fluorescence: Principles and Applications*, Wiley-VCH, Weinheim, 2002.
58. N. J. Turro, *Modern Molecular Photochemistry* University Science Books Sausalito, 1991.
59. A. Dadabhoy, S. Faulkner and P. G. Sammes, *Journal of the Chemical Society, Perkin Transactions 2*, 2002, DOI: 10.1039/b104541p, 348-357.
60. P. Caravan, J. J. Ellison, T. J. McMurry and R. B. Lauffer, *Chemical Reviews*, 1999, **99**, 2293-2352.

61. S. Aime, M. Botta, Z. Garda, B. E. Kucera, G. Tircso, V. G. Young and M. Woods, *Inorganic chemistry*, 2011, **50**, 7955-7965.
62. K. J. Miller, A. A. Saherwala, B. C. Webber, Y. Wu, A. D. Sherry and M. Woods, *Inorganic chemistry*, 2010, **49**, 8662-8664.
63. M. Woods, Z. Kovacs, R. Király, E. Brucher, S. Zhang and A. D. Sherry, *Inorganic chemistry*, 2004, **43**, 2845−2851.
64. S. Aime, M. Botta and G. Ermondi, *Inorg. Chem*, 1992, **31**, 4291-4299.
65. S. Aime, M. Botta, M. Fasano, M. P. M. Marques, C. F. G. C. Geraldes, D. Pubanz and A. E. Merbach, *Inorganic chemistry*, 1997, **36**, 2059-2068.
66. A. Takacs, R. Napolitano, M. Purgel, A. C. Benyei, L. Zekany, E. Brucher, I. Toth, Z. Baranyai and S. Aime, *Inorganic chemistry*, 2014, DOI: 10.1021/ic4025958.
67. A. K. R. Junker, M. Tropiano, S. Faulkner and T. J. Sørensen, *Inorganic chemistry*, 2016, **55**, 12299-12308.
68. A. Beeby, I. M. Clarkson, R. S. Dickins, S. Faulkner, D. Parker, L. Royle, A. S. de Sousa, J. A. G. Williams and M. Woods, *Journal of the Chemical Society, Perkin Transactions 2*, 1999, DOI: 10.1039/a808692c, 493-504.
69. M. Tropiano, O. A. Blackburn, J. A. Tilney, L. R. Hill, T. Just Sørensen and S. Faulkner, *J. Luminescence*, 2015, **167**, 296-304.
70. W. D. Horrocks and D. R. Sudnick, *Journal of the American Chemical Society*, 1979, **101**, 334-340.
71. G. E. BUONO-CORE, H. LI and B. MARCINIAK, *Coordination Chemistry Reviews*, 1990, **99**, 55-87.
72. N. Sabbatini, M. T. Indelli, M. T. Gandolfi and V. Balzani, *J Phys Chem-Us*, 1982, **86**, 3585-3591.
73. T. A. Shakhverdov, *Optics and Spectroscopy-USSR*, 1970, **29**, 166-169.
74. D. R Allan, H. Nowell, S. A. Barnet, M. R. Warren, A. Wilcox, J. Christensen, L. K. Saunders, A. Peach, M. T. Hooper, L. Zaja, S. Patel, L. Cahill, R. Mashall, S. Trimnell, A. J. Foster, T. Bates, S. Lay, M. A. Williams P. V. Hathaway, G. Winter, M. Gerstel and R. W. Wooley, Crystals, manuscript submitted
75. G. Winter, J. Appl. Cryst., 2010, 43, 186-190.
76. G. M. Sheldrick, Acta Cryst A, 2015, 71, 3-8
77. L. Palatinus, and G. Chapuis, J. Appl. Cryst., 2007, 40, 786-790
78. P. W. Betteridge, J. R. Carruthers, R. I. Cooper, K. Prout and D. J. Watkin, J. Appl. Cryst., 2003, 36, 1487
79. P. Parois, R. I. Cooper and A. L. Thompson, Chemistry Central Journal, 2015, 9:30
80. R. I. Cooper, A. L. Thompson and D. J. Watkin, J. Appl. Cryst., 2010, 43, 1100-1107
81. A. Spek, J. Appl. Cryst. (2003)
82. P. van der Sluis & A. L. Spek, Acta Cryst. (1990), A46, 194-201